Rheological Behavior of Polypropylene/Layered Silicate Nanocomposites Prepared by Melt Compounding in Shear and Elongational Flows

Seung Hwan Lee, EunNaRi Cho, Jae Ryoun Youn

School of Materials Science and Engineering, Seoul National University, Gwanak-Gu, Seoul 151-742, Korea

Received 29 March 2006; accepted 25 July 2006
DOI 10.1002/app.25204
Published online in Wiley InterScience (www.interscience.wiley.com).

ABSTRACT: Melt rheology and processability of exfoliated polypropylene (PP)/layered silicate nanocomposites were investigated. The nanocomposites were prepared by melt compounding process in the presence or absence of a PP-based maleic anhydride compatibilizer. PP/layered silicate nanocomposites showed typical rheological properties of exfoliated nanocomposites such as nonterminal solid-like plateau behavior at low frequency region in oscillatory shear flow, higher steady shear viscosity at low shear rate region, and outstanding strain hardening behavior in uniaxial elongational flow. The melt processability of exfoliated PP/layered silicate nanocomposites was significantly improved due to good dispersion of layered silicates and increased molecular interaction between the PP matrix and the layered silicate organoclay. Small-angle X-ray scattering and transmission electron microscopy results revealed that the layered silicate organoclay was exfoliated and good interaction between PP matrix and organoclay was achieved by using the PP-*g*-MAH compatibilizer.
 J Appl Polym Sci 103: 3506–3515, 2007

Key words: nanocomposites; melt rheology; processability; shear flow; elongational flow; compatibilizer; organoclay

INTRODUCTION

Polypropylene (PP) is a thermoplastic material that is produced by polymerizing propylene monomers into very long polymer molecules or chains. It is one of the fastest growing commodity resins in the polymer world market. It has many desirable properties such as: high melting point, low density, high tensile modulus, and low cost.[1] Conventional linear PP, however, has poor melt strength (MS) and weak strain hardening behavior in elongational flow. Therefore, it cannot be used easily in manufacturing processes where elongational flows are dominant, such as: foaming, blow molding, extrusion coating, and fiber spinning. It is expected that the improvement of the strain hardening behavior and MS of PP will contribute to the growth of this polymer in the plastics market. For this reason, many plastic makers are developing high MS of PP.[2–4]

The MS of PP can be improved by increasing the molecular weight, broadening the distribution, or by introducing branches. One of the effective approaches to achieve the high MS is adding long chain branches or grafting to backbone molecules. It is possible to crosslink PP by irradiation of electron beams and by adding peroxides. The PP branching or grafting yields high MS and strain hardening behavior. The modification increases molecular weight distribution owing to the radicals formed simultaneously in polymer materials.[5–9]

On the other hand, polymer nanocomposites have recently attracted great interest since they frequently exhibit unexpected hybrid properties synergistically derived from two components. One of the most promising composites would be hybrid systems based on organic polymer and inorganic clay minerals consisting of layered silicates.[10,11] The polymer/layered silicate nanocomposite is a typical example of polymer nanocomposites. Smectite-type clays, such as: hectorite, synthetic mica, and montmorillonite, are employed as fillers to enhance the mechanical and thermal properties of polymer matrix. The nanocomposites exhibit superior properties such as: enhanced mechanical properties,[12] reduced gas permeability,[13] and improved biodegradability.[14] The improved properties depend on the dispersion and orientation of the highly anisotropic clays in the polymer matrix.

The exfoliated and homogeneous dispersion of the silicate layers, however, could be achieved only in a few cases, e.g., polymers containing polar functional groups. This is mostly due to the fact that the silicate layers of the clay have polar hydroxy groups and are compatible only with polymers containing polar functional groups. Since PP does not include any polar groups in its backbone, it has been expected that

Correspondence to: J. R. Youn (jaeryoun@snu.ac.kr).
Contract grant sponsor: Korea Science and Engineering Foundation.

Journal of Applied Polymer Science, Vol. 103, 3506–3515 (2007)

the homogeneous dispersion of the silicate layers in the PP would not be realized. According to recent reports,[15–18] it was shown that the exfoliated PP/layered silicate nanocomposites were prepared by particular combination of PP, organoclay, and compatibilizer using the melt compounding process. Wang et al.[19] reported on the effects of compatibilizer type and feeding sequence on PP/layered silicate nanocomposites when they were compounded in a twin-screw extruder. Paul and coworkers[20] demonstrated the importance of the surface chemistry of the organoclay surface and how the organoclay was dispersed into the molten thermoplastic polymers. In particular, they paid a great attention to PP-based nanocomposites prepared by the melt compounding process. Okamoto and coworkers[21] demonstrated the hierarchical structure of the exfoliated PP/layered silicate nanocomposites by comparing the scale of the molecular structure, i.e., PP-*g*-MAH chains confined in the space of the silicate galleries with the width of 2–3 nm, crystalline lamellae with the thickness of 7–15 nm, and spherulitic texture with the diameter of 10 μm. They also reported that the real space in the house of cards structure formed under the elongational flow was observed by transmission electron microscopy (TEM) analysis. Both strong strain hardening and rheopexy features are originated from the alignment of the silicate layers perpendicular to the flow direction. Galgali et al.[22] conducted rheological study on the kinetics of hybrid formation in PP nanocomposites and found that the compatibilizer has a significant influence on modifying the rheological behavior.

However, it has not been completely understood how the compatibilizer and organoclay affect the uniaxial elongational behavior and processability of PP/layered silicate nanocomposites. It is necessary to understand various rheological properties and processability of nanocomposites prepared by melt compounding in the presence or absence of a PP-based maleic anhydride compatibilizer. Therefore, in this study, the exfoliated PP/layered silicate nanocomposites were prepared by melt compounding and the effects of morphology and molecular structure on melt rheology and processability were investigated.

EXPERIMENTAL

Materials

The isotactic PP homopolymer for sheet extrusion (HP550K, MFI 3.5 g/10 min, Polymirae, Seoul, Korea) was used as the base polymer resin. The organoclay was a natural montmorillonite modified with a quaternary ammonium salt (Cloisite®15A, Southern Clay, TX) via ion-exchange reaction. Maleic anhydride grafted PP (Polybond®3150, Crompton, TX) with the *g*-MAH content of 0.50 wt % was used as the compatibilizer.

Preparation of nanocomposites

All samples were prepared by melt compounding in a count-rotating twin-screw extruder (Brabender PLASTICORDER PLE-651). Melt compounding was carried out at 190°C and at the screw speed of 100 rpm with five different organoclay contents of 1, 3, 5, 7, and 10 wt %. The compounded melt was water quenched and pelletized. For rheological measurements the pellets were compression molded into a disk of 25 mm diameter and 1.5 mm thickness. For the elongational rheological measurements, the pellets were compression molded into a rectangular strip of 57.0 × 7.0 × 1.5 mm^3. Compositions of the prepared samples are listed in Table I.

Characterization

Small-angle X-ray scattering (SAXS) was conducted on a Rigaku Max-3 X-ray diffractometer with Cu–Kα radiation of wavelength 0.154 nm to determine the structure of layered silicate nanocomposites. The diffraction angle was varied as 0°–8°. TEM (JEOL JEM-2000EXII) was used for direct observation of the layered silicate organoclay structure in the nanocomposites. The specimens were prepared using an Ultracut E (Reichert) microtome. Thin sections of about 100 nm thickness were cut with a Diatome diamond knife at room temperature and coated with carbon for 5 min to prevent them from degradation caused by the irradiation of electrons.

Steady shear flow measurements were carried out using two types of rheometer. Rotational (AR-2000, Rheometric Scientific) and capillary (Rheograph-2003, Göttfert) rheometers were used at low and high shear rates, respectively. Parallel plate geometry

TABLE I
Compositions of the Prepared Nanocomposites Based on Pure Polypropylene, PP-*g*-MAH Compatibilizer, and Organoclay (wt %)

Sample	PP (wt %) (HP550K)	PP-*g*-MAH (wt %) (Polybond®3150)	Organoclay (wt %) (Closite 15A)
Pure PP	100	0	0
iPP/0/5[a]	95	0	5
iPP/5/5[b]	90	5	5
iPP/5/1	94	5	1
iPP/5/3	92	5	3
iPP/5/7	88	5	7
iPP/5/10	85	5	10
iPP/10/5	85	10	5
iPP/10/10	80	10	10

[a] Uncompatibilized nanocomposite.
[b] PP-*g*-MAH-compatibilized nanocomposite.

was used to measure the steady shear viscosity with respect to shear rates of 0.001–10 s^{-1}. In the parallel plate instrument, two plates with the diameter of 25 mm and the gap size of 1.0 mm used. Capillary rheometer was used to measure the steady state shear viscosity with respect to shear rate of 10–1000 s^{-1}. A capillary with the diameter of 1.0 mm and L/D ratio of 30 was used and measurements were carried out at 190°C. Dynamic oscillatory shear flow measurements were conducted using a rotational rheometer (AR-2000, Rheometric Scientific) with parallel plates. Frequencies of 0.01–200 rad/s were used at the strain amplitude of 10% to be within the linear viscoelastic region. Stress relaxation measurements were performed using a controlled strain rheometer (ARES, Rheometric Scientific) with a parallel plate shear flow device with the strain of 5%. In these experiments, parallel plates with the diameter of 25 mm and the gap size of 1.0 mm were used.

The viscosity growth during uniaxial elongational flow at a constant extension rate was measured using a Meissner-type elongational rheometer (RME®, Rheometric Scientific). A sample of rectangular cross section is elongated between two rotating clamps. A constant speed of the two clamps make it possible to deform the melt homogeneously and to apply a constant elongation rate to the polymer melts. Instead of using a silicone oil bath to keep the temperature constant and to compensate the sample weight, the melt is suspended by nitrogen gas. The constant extension rates were applied at elongation rates of 0.05, 0.1, 0.3, 0.5, and 1.0 s^{-1}. The transient elongational viscosity $\eta(t)$ is given by

$$\eta(t) = \frac{\sigma(t)}{\dot{\varepsilon}_0} = \frac{F(t)}{H_0 W_0 \exp[-\dot{\varepsilon}_0 t]\dot{\varepsilon}_0} \quad (1)$$

where, H_0 and W_0 are the thickness and width of the sample at $t = 0$, and $\dot{\varepsilon}_0$ is the elongational strain rate. The product H_0W_0 represents the cross-sectional area of the sample at the measurement temperature prior to extension and can be determined from the dimensions of the sample at room temperature. The extensional force produced by the sample is measured directly by a transducer linked to the right clamp.

Processability

Processability of the nanocomposite melt was investigated by measuring the MS and melt flow index (MFI) of the samples after melt compounding. The MS measurement was conducted using a fiber spinning device (Rheotens®, Göttfert) in combination with a capillary rheometer (RH-7, Rosand). A capillary with the diameter of 2.0 mm and the L/D ratio of 16 was used. The MS was measured after keeping the samples at constant temperatures of 190°C for 10 min. The extruded strand velocity at die exit and the take-up velocity were 46.9 and 250 mm/s, respectively. The distance from the die to the take-up wheel was 85 mm and the force was measured at a constant velocity of 250 mm/s. The MFI of various samples was measured by weighing the run PP for 10 min under 2.16 kg at 230°C using a melt flow indexer (Melt Flow Indexer, Göttfert).

RESULTS AND DISCUSSION

Morphology

There are two types of polymer/layered silicate nanocomposites, either intercalated or exfoliated, depending on the degree of separation of the individual organoclay platelets. When organoclay is blended with the polymer resin and the silicate layers do not separate, it is referred as a conventional composite material. In the intercalated structure polymer chains enter the clay galleries and cause the platelets separated apart less than 20–30 Å. In the exfoliated structure the silicate layers are delaminated and dispersed well in the polymer matrix.[23] Figure 1 SAXS patterns in the range of $2\theta = 0^o$–8^o for organoclay powders, uncompatibilized composites (iPP/0/5), and PP-*g*-MAH compatibilized nanocomposites (iPP/5/5, iPP/5/10). The SAXS pattern of the original organoclay shows the peak of intensity at the diffraction angle of $2\theta = 2.65^\circ$ and the equivalent distance between silicate layers is 34.46 Å. The SAXS spectra of PP-*g*-MAH compatibilized nanocomposites do not show the characteristic basal reflection of the organoclay. This is possibly a direct evidence of the exfoliation because the peak of organoclay around $2\theta = 2.65^\circ$ disappeared. The SAXS results imply that the fully exfoliated struc-

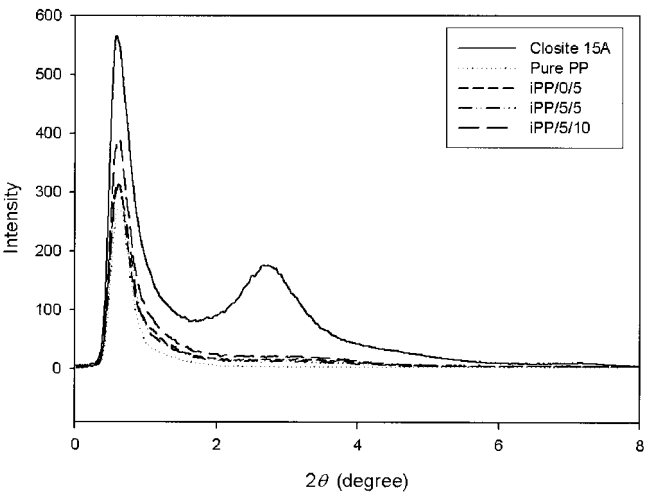

Figure 1 SAXS patterns of organoclay powder, pure PP, uncompatibilized nanocomposite (iPP/0/5), and two types of compatibilized nanocomposites (iPP/5/5 and iPP/5/10).

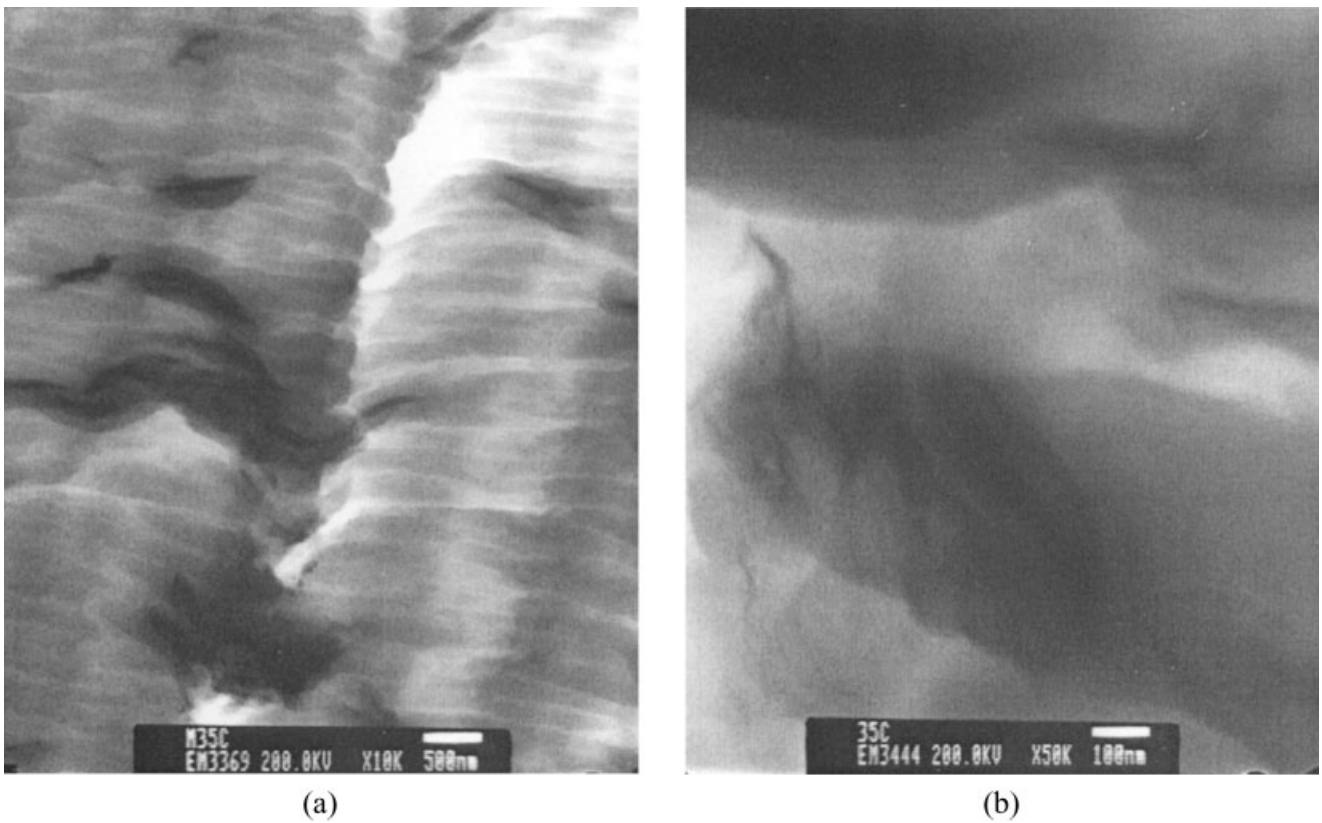

Figure 2 TEM images of (a) at low (×10,000) and (b) at high (×50,000) magnification of uncompatibilized nanocomposite (iPP/0/5) prepared by the twin-screw extruder.

ture was generated during the melt extrusion process. However, SAXS spectra patterns of the organoclay filled PP nanocomposites display a slight increase in the intensity at lower 2θ values when compared with that of the unfilled polymer matrix. In addition, the peak at $2\theta = 2.65^\circ$ disappeared for the uncompatibilized composite because the SAXS measurement examined the microsturcture in a limited region of samples and the concentration of the organoclay was low. Because the melt rheology result shows the macrostructural properties of a large volume, TEM observation and rheological behavior of the nanocomposite should be considered together with the SAXS data for proper interpretation.

To observe the exfoliated structure of the silicate layers, TEM images for uncompatibilized composites and compatibilized nanocomposites prepared with different organoclay and compatibilizer loadings are shown in Figures 2 and 3. Figure 2(a, b) show TEM images of the uncompatibilized composite (iPP/0/5) at low (10,000×) and high (50,000×) magnification. In the case of uncompatibilized composites the silicate layers were aggregated with a size of several hundreds of nanometers in the PP matrix. Figures 3(a) and (b) show TEM images for nanocomposites containing organoclay of 10 wt % and compatibilizer of 10 wt % (iPP/10/10). The micrograph of the PP-*g*-MAH compatibilized nanocomposite shows that individual exfoliated platelets are embedded in the polymer matrix resin. Each layer of the organoclay is dispersed homogeneously in the PP matrix, although a small amount of intercalated layers still exists. It is apparent that the PP-*g*-MAH compatibilizer improved the dispersity and homogeneity of layered silicates in PP matrix.

Shear flow

Viscoelastic response of nanocomposites upon application of a steady shear flow plays an important role for evaluation of the melt processability. To enhance processability of PP/layered silicate nanocomposites, rheological behavior of the nanocomposites in molten state should be understood in detail. Rheological properties of the nanocomposites are also helpful in understanding morphology–property relationships.

In Figure 4, the steady state shear viscosity was measured with rotational and capillary rheometers and plotted as a function of shear rate for pure PP, uncompatibilized composites, and PP-*g*-MAH compatibilized nanocomposites at 190°C. While the pure PP, uncompatibilized composites, and nanocomposites containing organoclay of 1 wt % (iPP/5/1) exhibit Newtonian behavior at low shear rates (1 s^{-1})

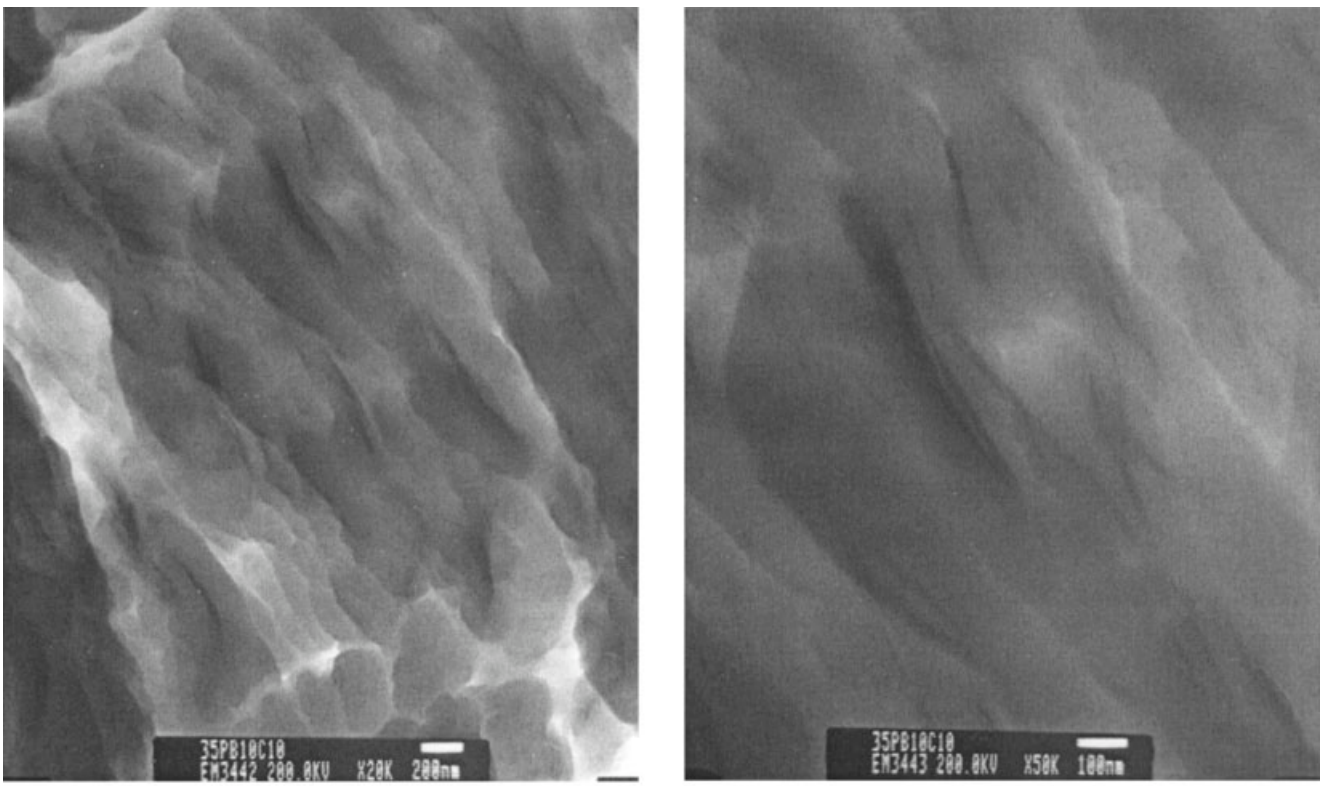

Figure 3 TEM images of (a) at low (×20,000) and (b) at high (×50,000) magnification of compatibilized nanocomposite (iPP/10/10) prepared by the twin-screw extruder.

and power-law behavior at high shear rates (above 10 s^{-1}), PP-*g*-MAH compatibilized nanocomposites (organoclay of above 3 wt %) exhibited non-Newtonian behavior at all shear rate regions. Especially, the steady shear viscosity of the compatibilized nanocomposites (iPP/5/5) initially exhibit shear-thickening behavior at low shear rate region. According to Okamoto and coworkers,[24] one possible explanation for this behavior may involve planar alignment of the organoclay particles in the flow direction under shear force. For a very slow shear rate (0.001 s^{-1}), it takes a longer time for organoclay particles to attain complete planar alignment in the flow direction and hence shear-thickening behavior is observed. By contrast, at higher shear rates (0.005 or 0.01 s^{-1}) the measurement time is long enough to attain such alignment and hence the nanocomposites show a time-independent shear viscosity. Subsequently, PP-*g*-MAH compatibilized nanocomposites show very strong shear thinning behavior at all shear rates. Additionally, viscosities of the nanocomposites are comparable with that of pure PP matrix at very high shear rates. These observations suggest that the silicate layers are strongly oriented in the flow direction at high shear rates and that the shear thinning behavior observed at high shear rates is dominated by that of pure polymer matrix.

Key viscoelastic parameters can be measured in small amplitude oscillation as a function of strain, stress, frequency, time, or temperature. Figure 5 illustrates the storage modulus obtained from strain sweep tests at the angular frequency of 6.28 rad/s on the pure PP, uncompatibilized nanocomposites, and PP-*g*-MAH compatibilized nanocomposites. A strain

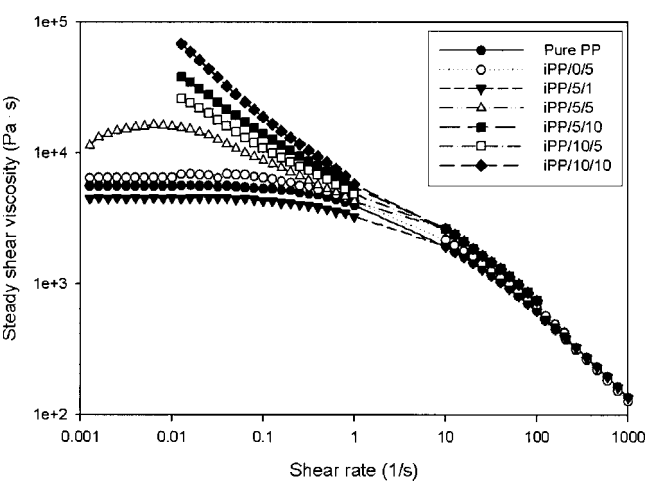

Figure 4 Shear viscosity as a function of shear rate for pure PP, uncompatibilized nanocomposite (iPP/0/5), and compatibilized nanocomposites at $T = 190°C$.

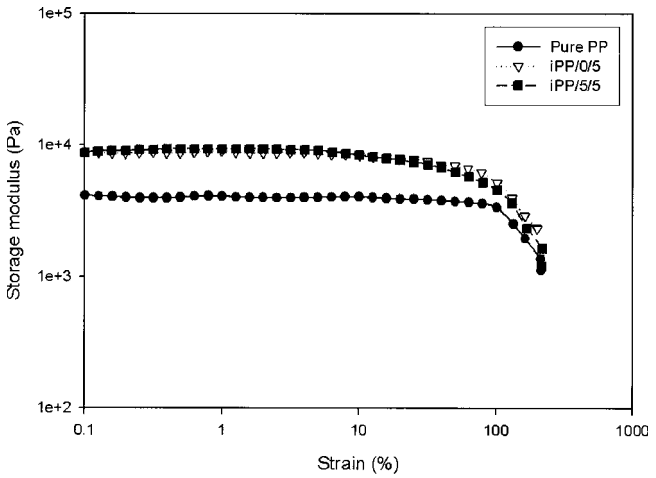

Figure 5 Storage modulus (G') as a function of strain for the pure PP (iPP), uncompatibilized nanocomposite (iPP/0/5), and compatibilized nanocomposite (iPP/5/5) at $T = 190°C$.

sweep dynamic test in which the sample is subject to increasing oscillatory strain at controlled frequency can differentiate the linear and nonlinear regimes and investigate dispersion stability. In the linear region, the material responds linearly to the strain and the structure remains unchanged. The transition from the linear to the nonlinear regime, characterized by the rapid decrease in storage modulus (G'), occurs at about the strain of 100% for the pure PP. For the compatibilized and uncompatibilized samples the transition occurs much earlier at the strain of about 50%. Further rheological characterizations in the linear regime were done at the strain of 10% for all samples.

Storage (G') and loss (G'') moduli are plotted in Figure 6 with respect to the angular frequency (ω) for pure PP, uncompatibilized nanocomposites, and compatibilized nanocomposites. The pure PP shows classical viscoelastic behavior, namely, a terminal flow regime where G' and G'' are proportional to ω^2 and ω, respectively. The uncompatibilized nanocomposite shows a small deviation from classical behavior in the case of G' and G'' at lower frequencies. However, oscillatory behaviors of the compatibilized nanocomposites are distinctly different. At low frequency region, storage modulus (G') shows nonterminal plateau solid-like behavior and has higher value in comparison with that of pure PP or uncompatibilized nanocomposites. The nonterminal behavior of the nanocomposite is similar to that reported earlier for other intercalated polymer/layered silicate nanocomposites,[25] particle-filled polymer melts,[26] or long-chain branched polymer melts.[27] At high frequency, the values of storage modulus for compatibilized nanocomposites are similar to that of pure PP matrix, indicating that segmental motion of the polymer matrix determines the material response at short time scales.

In Figure 7, the complex viscosity (η^*) is plotted as a function of frequency for several samples at 190°C. Stronger and earlier shear thinning behaviors were observed in the PP-*g*-MAH compatibilized nanocomposites at low frequency region. It is also seen that organoclay contents increase the magnitude of the viscosity especially in the low frequency region. It is obvious that the PP-*g*-MAH compatibilized nanocomposites have higher complex viscosity than pure PP or uncompatibilized nanocomposites.[27]

Figure 8 shows the steady shear viscosity and the complex viscosity for pure PP, uncompatibilized nanocomposites, and PP-*g*-MAH compatibilized nanocomposites. A correlation between steady and oscillatory

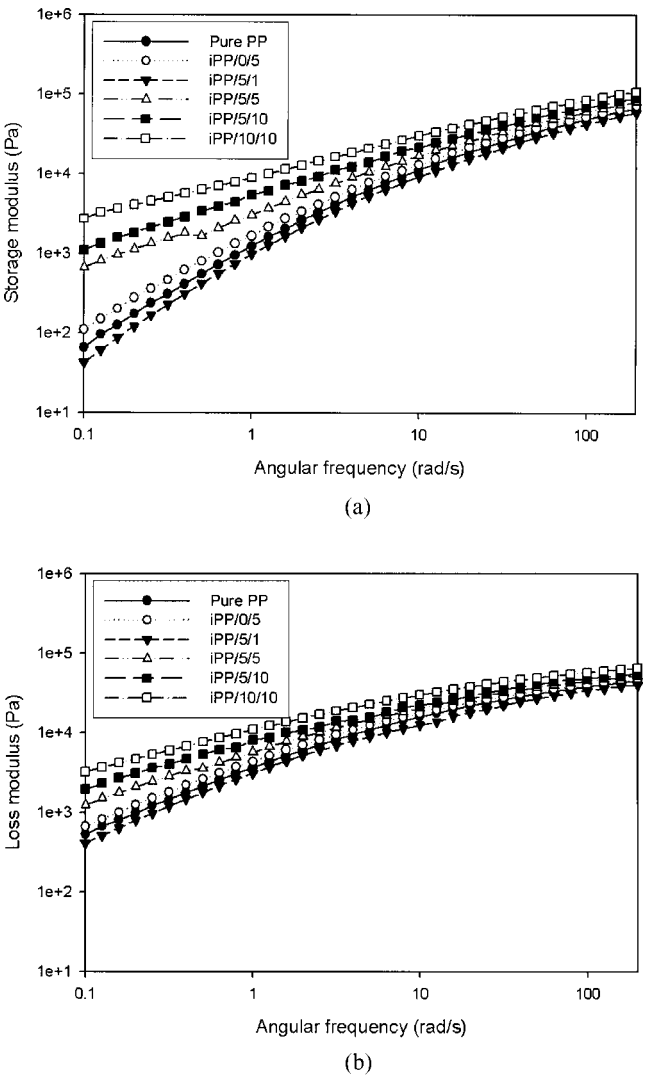

Figure 6 Frequency dependence of (a) storage modulus (G') and (b) loss modulus (G'') curves for the pure PP, uncompatibilized nanocomposite, and various compatibilized nanocomposites at $T = 190°C$.

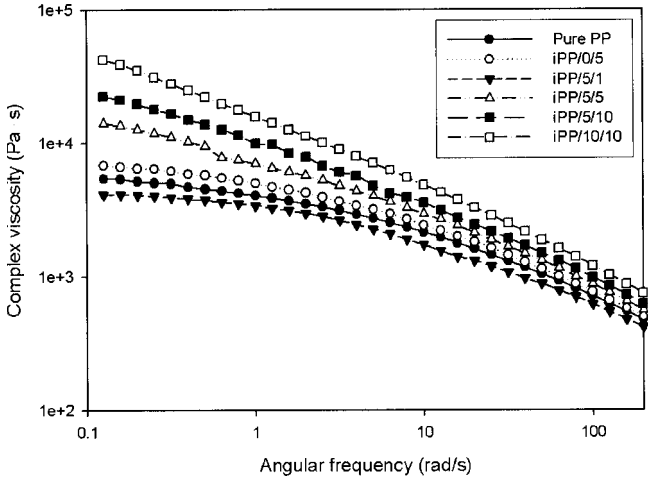

Figure 7 Complex viscosity curves for the pure PP, uncompatibilized nanocomposite, and various compatibilized nanocomposites at $T = 190°C$.

flow behaviors for flexible chain homopolymer was given by the empirical equation of Cox and Merz,[28]

$$\eta(\dot{\gamma}) = \eta^*(\omega)|_{\omega=\gamma} \quad (2)$$

where, $\eta(\dot{\gamma})$ is the steady state shear viscosity measured at a steady shear rate of $\dot{\gamma}$ and $\eta^*(\omega)$ is the complex viscosity at an oscillatory frequency of ω. For the pure PP and uncompatibilized composite, the agreement is quite good. However, the complex viscosity is much greater than the shear viscosity in the PP-*g*-MAH compatibilized nanocomposite. Generally, polymer/layered silicate nanocomposites always exhibit significant deviations from the Cox–Merz rule, while all pure polymers obey the empirical relation. According to previous reports,[29] two possible reasons were offered for the deviation from the Cox–Merz rule in the case of nanocomposites. First, Cox–Merz rule is only applicable for homogenous systems like homopolymer melts, but nanocomposites are heterogeneous systems. Second, the structure formation is different when nanocomposites are subject to dynamic oscillatory shear and steady shear measurements. The resistance to flow for small amplitude oscillatory flow is much larger than that for steady shear flow where shear strain in increasing continuously. This is clearly associated with forces between the particles of the organoclay network.

Figure 9 shows the experimentally determined linear relaxation modulus, $G(t)$, of pure PP, uncompatibilized composites, and PP-*g*-MAH compatibilized nanocomposites. It is observed that, for any fixed time after the imposition of strain, the modulus $G(t)$ increases with silicate loading, as in the case of dynamic oscillatory shear measurement. Theoretical prediction of the linear relaxation modulus is compared with experimental results, obtained at $\gamma_0 = 0.05$. The solid line represents the relaxation modulus in the linear regime which can be calculated by a sum of exponential functions as

$$G(t) = \sum_{i=1}^{N} G_i \exp(-t_i/\tau_i) \quad (3)$$

where G_i and τ_i are the i-th relaxation time and corresponding modulus, respectively, determined from dynamic oscillatory shear measurement.[30] It is important for calculation of the relaxation modulus that N should be sufficiently large for precise quantitative fitting. There is a good agreement between the predicted and measured values of the relaxation modulus because linear relationship is effective in both dynamic

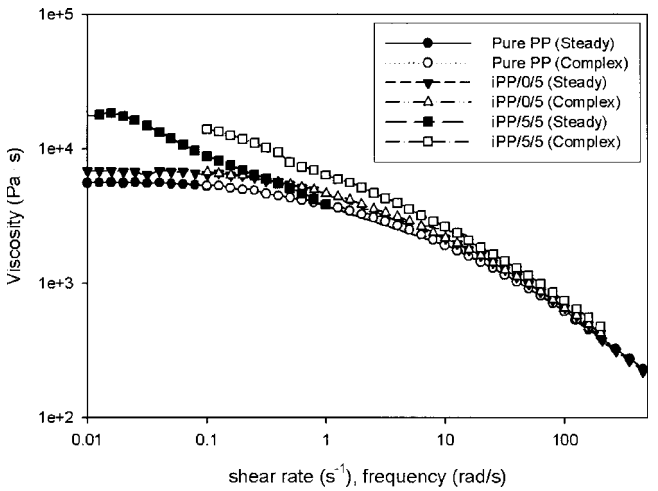

Figure 8 Comparison between the steady and dynamic shear viscosity curves for the pure PP, uncompatibilized nanocomposite (iPP/0/5), and compatibilized nanocomposite (iPP/5/5).

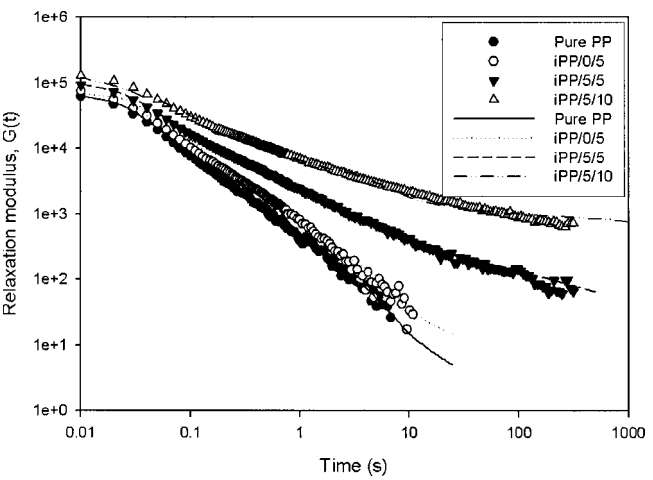

Figure 9 Experimental (symbol) and predicted (solid line) linear relaxation modulus $G(t)$ for the pure PP, uncompatibilized composite (iPP/0/5), and two types of compatibilized nanocomposites (iPP/5/5, iPP/5/10) at $\gamma = 0.05$.

oscillatory shear and stress relaxation modes. The linear relaxation modulus of the compatibilized nanocomposite is much larger than that for pure PP or uncompatibilized composites. Compatibilized nanocomposites relax like a solid material while the pure PP and uncompatibilized composite relax quickly. Both the dynamic oscillatory shear and the stress relaxation moduli indicate that the addition of the layered silicate and compatibilizer to PP resin significantly modifies the long-time relaxation behavior of the nanocomposites by increasing the relaxation time due to the formation of a three-dimensional network structure.[31] Kotsilkova[32] suggested that longer relaxation time and larger relaxation modulus of the compatibilized nanocomposite indicate that the two phase of the structure of nanocomposite creates a significant energetic barrier against the molecular motion during the shear flow. It is probably due to both the presence of multilayered clay domains dispersed on a molecular level in the PP matrix and the interfacial interaction between polymer chains and silicate surfaces.

Elongational flow

Okamoto et al.[33] first conducted elongational flow tests of PP/layered silicate nanocomposite in the molten state at constant elongational rate ($\dot{\varepsilon}_0$) using an elongation rheometer. Figure 10 shows double logarithmic plots of the transient elongational viscosity growth functions, $\eta_E(\dot{\varepsilon}_0, t)$, observed for pure PP at 190°C with different elongational rates ranging from 0.05–1.0 s^{-1}. The elongational viscosity increases linearly with time and does not reach a steady state. Also strain-induced hardening was not observed in this case. Figure 11 shows the transient elongational viscosity growth of the uncompatibilized composite. As in the case of pure polymer matrix, conventional composites without the compatibilizer did not exhibit any strain hardening behavior in molten state.

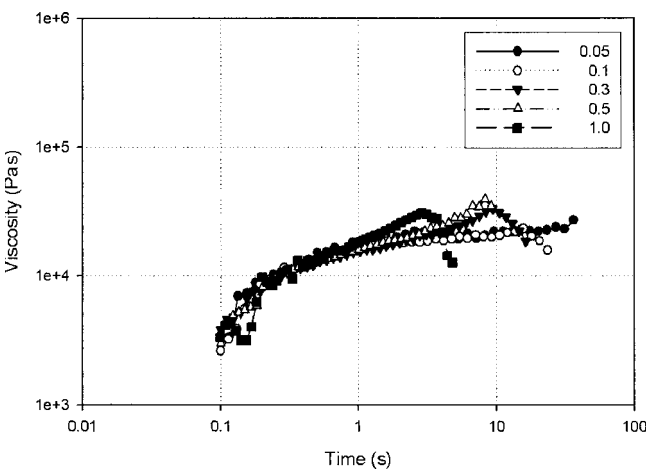

Figure 10 Elongational viscosity growth curves of pure PP melts at different elongational strain rates ($T = 190$°C).

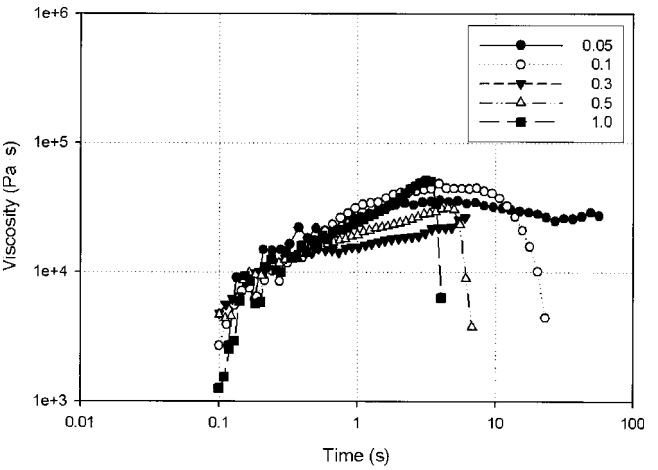

Figure 11 Elongational viscosity growth curves of uncompatibilized nanocomposite (iPP/0/5) melts at different elongational strain rates ($T = 190$°C).

Figure 12 shows transient viscosity growth of the compatibilized nanocomposite. The initial part of all the elongational viscosity growth curves showed simple monotonic growth that agreed well with the theory of linear viscoelasticity.[30] After deformation equivalent to the Hencky strain of about 1.0, however, some of the growth curves showed increase in the slope as the viscosity growth rate was accelerated, i.e., strain hardening. The compatibilized nanocomposite showed strong strain hardening behavior at different extension rates. The compatibilizer interplays between PP matrix and organoclay particles, and subsequently increases the flow resistance in uniaxial elongational flow. The elongational viscosity of the linear PP did not show strain hardening. The three-dimensional network structure that was gener-

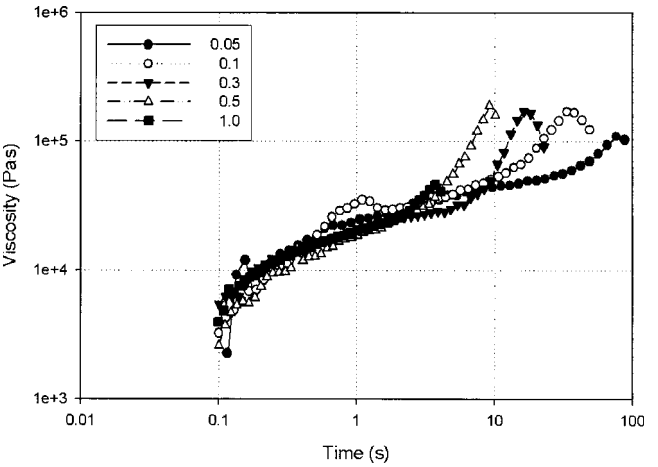

Figure 12 Elongational viscosity growth curves of compatibilized nanocomposite (iPP/5/5) melts at different elongational strain rates ($T = 190$°C).

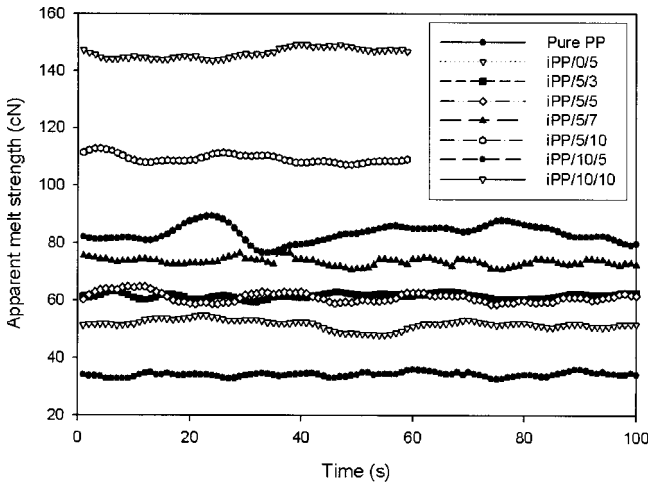

Figure 13 Apparent MS as a function of time for the pure PP, uncompatibilized nanocomposites, and several nanocomposites with different organoclay loadings.

ated during the melt compounding, however, increased the possibility of entanglement in the melt and reduced the rate of disentanglement. In general, the more networking added on the chains, the higher the strain hardening. The compatibilized nanocomposites showed enhanced strain hardening of their viscosities in uniaxial elongational flow. It is believed that the strain hardening behavior will be related to the processability such as higher MS or lower MFI of nanocomposites.[34]

Processability

Figure 13 shows the results of MS measured using Göttfert fiber spinning device. The compatibilized nanocomposite gives the MS of around 78 cN under the present experimental conditions. In particular, a nanocomposite melt with the organoclay of 10 wt % gives the MS of 112 cN which is higher than 38 cN of the pure PP. It is inferred that the PP-*g*-MAH compatibilizer used in nanocomposite production is responsible for the higher strain hardening and improved MS.

Table II shows the MFI of prepared samples after melt compounding. A linear trend can be seen between MS and MFI as shown in Figure 14. The MFI values decreased in the presence of PP-*g*-MAH compatibilizer. This may be attributed to higher reactivity of the maleic anhydride group generated in the formation of a graft polymer. The intermolecular bonding in the PP matrix may restrict the movement of the polymeric chains and affect the melt flow and viscosity. When the PP-based compatibilizer was added to the nanocomposite, the anhydride group would react with the terminal group of the organoclay during melt extrusion. Therefore, incorporation of the maleic anhydride group in the compatibilized nanocomposite slightly increased the melt viscosity and decreased the MFI. These interactions reduce the chain mobility and yield lower MFI values.

CONCLUSION

PP/layered silicate nanocomposites were prepared by melt compounding using PP-*g*-MAH compatibilizer to investigate morphology, rheology and processability of exfoliated nanocomposite melts. PP/layered silicate nanocomposites showed typical rheological properties of exfoliated nanocomposites such as nonterminal solid-like plateau behavior at low frequency region and higher steady shear viscosity at low shear rate region. Melt rheology of the compatibilized nanocomposite indicates that the microstructure consists of a percolating three-dimensional network of dispersed organoclays at low shear rates and small amplitude oscillatory shear flow. At high shear rates, the network breaks and the material shows yield behavior. PP/layered silicate nanocomposites showed outstanding strain hardening behavior and increased melt processability in uniaxial elongational flow. The strain hardening has been attributed to good dispersion of layered silicates and molecular interaction among the PP matrix, layered silicates, and compatibilizer. The intermolecular

TABLE II
Averaged Melt Strength and MFI after Melt Compounding with Brabender Twin Screw Extruder (T = 190°C, 100 rpm)

Sample	Pure PP (wt %)	PP-*g*-MAH (wt %)	Organoclay (wt %)	MFI (g/10 min)	Melt strength (cN)
Pure PP	100	0	0	5.455	52.3
iPP/0/5	95	0	5	5.144	61.2
iPP/5/5	90	5	5	4.650	66.7
iPP/5/1	94	5	1	7.016	Not measured
iPP/5/3	92	5	3	5.792	34.4
iPP/5/7	88	5	7	4.381	73.7
iPP/5/10	85	5	10	3.441	107.7
iPP/10/5	85	10	5	4.210	82.5
iPP/10/10	85	10	10	2.690	146.4

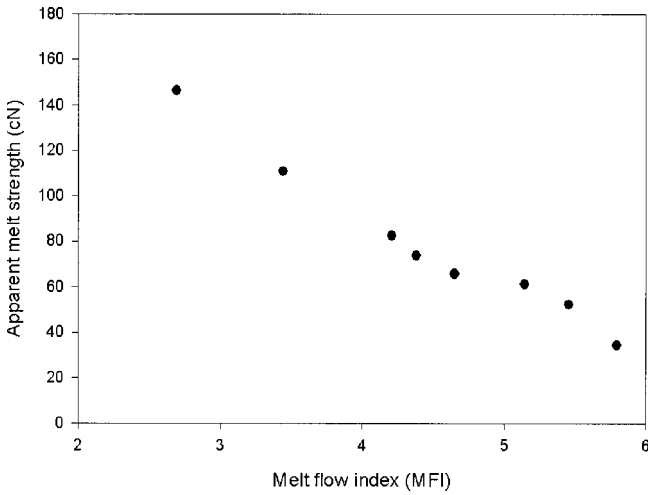

Figure 14 Apparent MS versus the MFI of pure PP, uncompatibilized nanocomposite (iPP/0/5), and various nanocomposites having different organoclay loadings.

bonding may restrict the movement of the polymeric chains in the PP resin and affect the melt flow and viscosity.

References

1. Karian, H. G. Handbook of Polypropylene and Polypropylene Composites; Marcel Dekker: New York, 2003.
2. Gabrel, C.; Munstedt, H. J Rheol 2003, 47, 619.
3. Gotsis, A. D.; Zeevenhoven, B. L. F.; Hogt, A. H. Polym Eng Sci 2004, 44, 973.
4. Kurzbeck, S.; Oster, F.; Munstedt, H.; Nguyen, T. Q.; Gensler, R. J Rheol 1999, 43, 359.
5. Zamotaev, P.; Chodak, I.; Mityukhin, O.; Chorvath, I. J Appl Polym Sci 1995, 56, 935.
6. Gotsis, A. D.; Zeevenhoven, B. L. F. J Rheol 2004, 48, 895.
7. Lagendijk, R. P.; Hogt, A. H.; Buijtenhuijs, A.; Gotsis, A. D. Polymer 2001, 42, 10035.
8. Sugimoto, M.; Tanaka, T.; Masubuchi, Y.; Takimoto, J.; Koyama, K. J Appl Polym Sci 1999, 73, 1493.
9. Rätzsch, M. Pure Appl Chem 1999, 36, 1759.
10. Ray, S. S.; Okamoto, M. Prog Polym Sci 2003, 28, 1539.
11. Pinnavaia, T. J.; Beall, G. W. Polymer-Clay Nanocomposites; Wiley-Interscience: New York, 2000.
12. Cho, J. W.; Paul, D. R. Polymer 2001, 42, 1083.
13. Xu, R.; Manias, E.; Snyder, A. J.; Runt, J. Macromolecules 2001, 34, 337.
14. Lee, S. K.; Seong, D. G.; Youn, J. R. Fibers Polym 2005, 6, 289.
15. Giannelis, E. P. Appl Organomet Chem 1998, 12, 675.
16. Zhang, Q.; Fu, Q.; Jiang, L.; Lei, Y. Polym Int 2000, 49, 1561.
17. Reichert, P.; Hoffmann, B.; Bock, T.; Thomann, R.; Mulhaupt, R.; Friedrich, C. Macromol Rapid Commun 2001, 22, 519.
18. Kim, K. N.; Kim, H.; Lee, J. W. Polym Eng Sci 2001, 41, 1963.
19. Wang, Y.; Chen, F.; Wu, K. J Appl Polym Sci 2004, 93, 100.
20. Dennis, H. R.; Hunter, D. L.; Chang, D.; Kim, S.; White, J. L.; Cho, J. W.; Paul, D. R. Polymer 2001, 42, 9513.
21. Nam, P. H.; Maiti, P.; Okamoto, M.; Kotaka, T.; Hasegawa, N.; Usuki, A. Polymer 2001, 42, 9633.
22. Galgali, G.; Ramesh, C.; Lele, A. Macromolecules 2001, 34, 852.
23. Zanetti, M.; Lomakin, S.; Camino, G. Macromol Mater Eng 2000, 279, 1.
24. Ray, S.; Okamoto, K.; Okamoto, M. Macromolecules 2003, 36, 2355.
25. Hyun, Y. H.; Lim, S. T.; Choi, H. J. Macromolecules 2003, 34, 8084.
26. Greener, J.; Evans, J. R. G. J Rheol 1998, 42, 697.
27. Kasehagen, L. J.; Macosko C. W. J Rheol 1998, 42, 1303.
28. Cox, W. P.; Merz, E. H. J Polym Sci 1958, 28, 619.
29. Krishnamoorti, R.; Giannelis, E. P. Macromolecules 1997, 30, 4097.
30. Ferry, J. D. Viscoelastic Properties of Polymers; Wiley-Interscience: New York, 1980.
31. Incarnato, L.; Scarfato, P.; Scartteia, L.; Acierno, D. Polymer 2004, 45, 3487.
32. Kotsilkova, R. Mech Time Depend Mater 2002, 6, 283.
33. Okamoto, M.; Nam, P. H.; Maiti, P.; Kotaka, T.; Hasegawa, N.; Usuki, A. Nano Lett 2001, 1, 295.
34. Chow, W. S.; Mohd Ishak, Z. A.; Karger-Kocsis, J.; Apostolov, A. A.; Ishiaku, U. S. Polymer 2003, 44, 7427.